International Journal of Nanomedicine

Dovepress
Taylor & Francis Group

Open Access Full Text Article

ORIGINAL RESEARCH

Utility of ^{131}I-HLX58-Der for the Precision Treatment: Evaluation of a Preclinical Radio-Antibody-Drug-Conjugate Approach in Mouse Models

Yi Liu[1–4,*], Xiao Wang[1–3,5,*], Ni Zhang[1–4,*], Simin He[1–4], Jianping Zhang[1–4], Xiaoping Xu[1–4], Shaoli Song[1–4]

[1]Department of Nuclear Medicine, Fudan University Shanghai Cancer Center, Shanghai, 200032, People's Republic of China; [2]Department of Oncology, Shanghai Medical College, Fudan University, Shanghai, 200032, People's Republic of China; [3]Center for Biomedical Imaging, Fudan University, Shanghai, 200032, People's Republic of China; [4]Shanghai Engineering Research Center of Molecular Imaging Probes, Shanghai, 200032, People's Republic of China; [5]State Key Laboratory of Vaccines for Infectious Diseases, Xiang an Biomedicine Laboratory & Center for Molecular Imaging and Translational Medicine, School of Public Health, Shenzhen Research Institute of Xiamen University, Xiamen University, Xiamen, 361102, People's Republic of China

*These authors contributed equally to this work

Correspondence: Shaoli Song; Xiaoping Xu, Department of Nuclear Medicine, Fudan University Shanghai Cancer Center, Shanghai, 200032, People's Republic of China, Email shaoli-song@163.com; xxp0012@ustc.edu

Purpose: None of the antibody-drug conjugates (ADCs) targeting Claudin 18.2 (CLDN18.2) have received approval from regulatory authorities due to their limited clinical benefits. Leveraging the radiosensitizing ability of Deruxtecan (DXd) and the internal radiation therapy of ^{131}I for tumors, we aimed to develop the first radio-antibody-drug conjugates (RADCs) for the treatment of gastric cancer.

Methods: The CLDN18.2-specific antibody HLX58 was conjugated with the payload DXd through a cleavable maleimide glycyn-glycyn-phenylalanyn-glycyn (GGFG) peptide linker. HLX58-Der was labeled with ^{131}I to produce RADC-^{131}I-HLX58-Der. HLX58 was labeled with ^{125}I for imaging CLDN18.2-positive tumors, providing a reference for RADC treatment in solid tumors. The antigen-binding properties and biodistribution of the RADC were studied both in vitro and in vivo. The cytotoxic effects of the RADC were evaluated in CLDN18.2-positive tumor cell lines and xenografts.

Results: HLX58 was successfully conjugated with DXd using the cleavable maleimide GGFG peptide linker and labeled with ^{131}I to produce RADC-^{131}I-HLX58-Der. HLX58 was labeled with ^{125}I for imaging CLDN18.2-positive tumors. Both ^{125}I-HLX58 and ^{131}I-HLX58-Der exhibited significant binding affinity for the CLDN18.2-positive cancer cell line. The cytotoxic effect of ^{131}I-HLX58-Der was observed in the CLDN18.2-positive cell line, with an IC_{50} of 11.28 ng/mL. In terms of cytotoxicity, ^{131}I-HLX58-Der exhibited greater activity compared to HLX58-Der. ^{125}I-HLX58 and ^{131}I-HLX58-Der demonstrated similar biodistribution profiles in CLDN18.2-positive tumor models, achieving 5.72 ± 0.41%ID/g (48 h) and 5.83 ± 0.41%ID/g (72 h) in the tumor tissues postinjection, respectively. The average tumor size in groups treated with ^{131}I-HLX58-Der and HLX58-Der was reduced by factors of 12.15 and 4.80, respectively, compared to the control group. ^{131}I-HLX58-Der demonstrated no toxic effects on hepatorenal function, routine blood tests, or major organs in mice when compared to the control group.

Conclusion: These findings validate the potential of RADCs targeting CLDN18.2 in treating CLDN18.2-expressing solid tumors.

Keywords: CLDN18.2, radio-antibody-drug conjugates, molecular imaging, precision medicine

Introduction

Gastric cancer (GC) ranks as the fifth most common malignant tumor and the fourth leading cause of cancer-associated deaths worldwide.[1,2] Notably, the incidence of gastric cancer among young adults (aged < 50 years) has progressively increased in recent years. Despite the high incidence of GC, most patients are unfortunately diagnosed at advanced

Received: 20 October 2024
Accepted: 9 January 2025
Published: 17 January 2025

Graphical Abstract

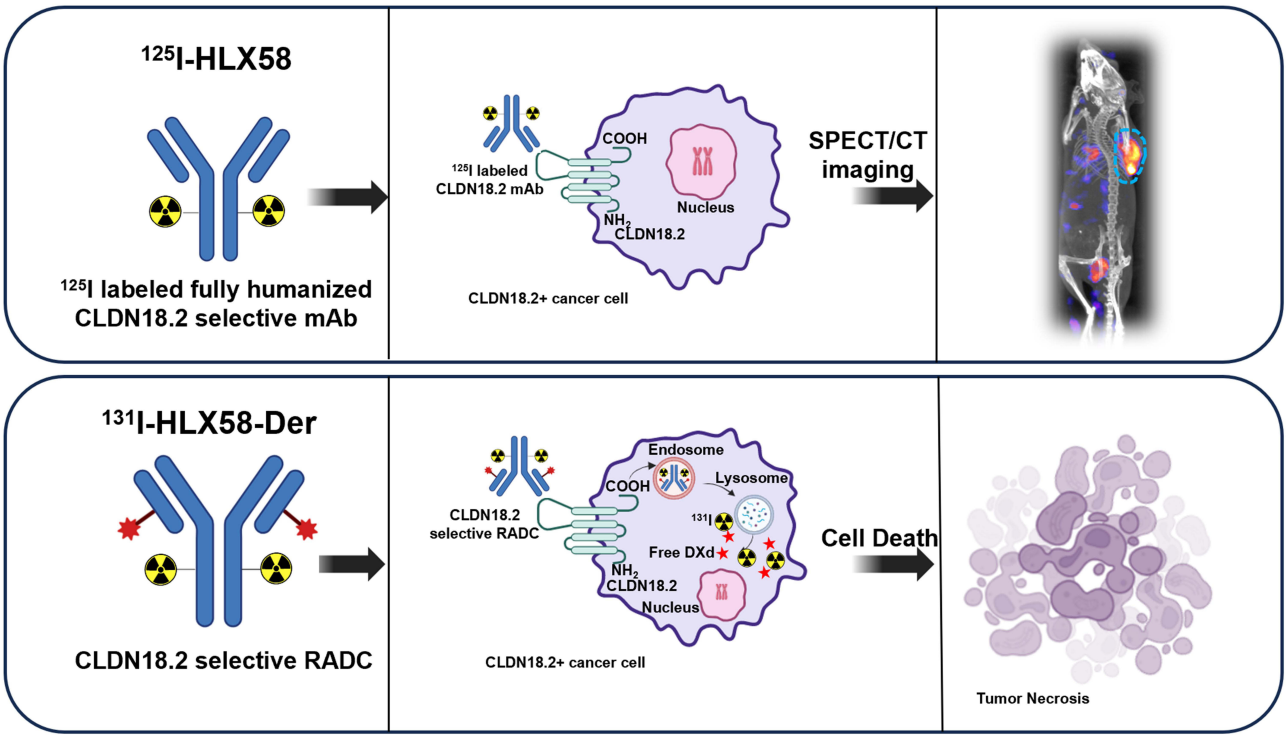

stages, resulting in a dismal prognosis due to the lack of distinguishing clinical indications.[3,4] Systemic chemotherapy remains the mainstay treatment for metastatic GC (mGC), with a median overall survival (OS) of approximately 12 months for patients receiving conventional chemotherapy.[5] Intratumoral and intertumoral heterogeneity are prominent features of GC that contribute significantly to its poor prognosis. Effective patients stratification is crucial for individualized treatment and improving clinical outcomes.[6] Therefore, cutting-edge diagnostic techniques and therapies are fundamentally important for accurately characterizing molecular profiles and identifying potential novel therapeutic targets for GC patients.[7–9]

Claudin 18 (CLDN18) is a highly specific tight junction protein encoded by the CLDN18 gene that regulates parallel barrier functions. CLDN18 has two isoforms, namely isoform 1 (CLDN18.1) and isoform 2 (CLDN18.2).[7] CLDN18.2 is exclusively present in the gastric mucosa and is retained during malignant transformation, making it an ideal candidate for monoclonal antibody binding with reduced off-target effects.[10] Antibodies targeting CLDN18.2 may serve as valuable tools for the precision treatment of gastric cancer.[11] Labeling CLDN18.2 antibodies with imaging radioisotopes enables real-time imaging of CLDN18.2 expression levels in tumor tissue. Furthermore, CLDN18.2 antibodies can accurately deliver therapeutic radioisotopes to tumor tissue, exerting a lethal effect on the target while minimizing damage to normal tissue.

Iodine can stably bind to antibodies via tyrosine. Iodine possesses multiple radioactive isotopes, including iodine-125 (^{125}I) and iodine-131 (^{131}I). ^{125}I is commonly used for imaging. ^{131}I is a classic therapeutic radioactive isotope that has been used for the treatment of thyroid cancer. CLDN18.2 can be labeled with ^{125}I or ^{131}I to form radionuclide-drug conjugates (RDCs) for the specific delivery of these radioisotopes. Targeted delivery of radioactive nuclides can achieve precise imaging and localized radiation to the target tissue, ensuring effective treatment while minimizing systemic exposure and radiation-induced toxicity to other tissues.[12] Meanwhile, based on the tripartite collaboration of CLDN18.2 antibody, an antitumor cytotoxic payload or warhead, and a suitable linker, antibody-drug conjugates (ADCs) are highly effective in killing tumor cells.[13,14] The payload of the HER2-targeting ADC (DS-8201a) is a derivative of DX-8951

(DXd), a novel topoisomerase I (TopI) inhibitor that demonstrates potent efficacy against various tumor xenograft models. DXd is bound to a maleimide glycynglycyn-phenylalanyn-glycyn (GGFG) peptide linker to form Deruxtecan. Therapy with trastuzumab deruxtecan resulted in significant improvements in response and overall survival compared to standard therapies among patients with HER2-positive GC.[15] Deruxtecan is classified within the Camptothecin family. As an antiproliferative agent, Deruxtecan can induce cell cycle arrest specifically in the G2/M phase. Cells in this phase are known to exhibit increased sensitivity to radiation.[16]

ADCs represent an innovative treatment for several cancers due to their high specificity, strong selectivity, promising clinical efficacy, and reduced likelihood of toxicity. Currently, nine ADCs have been approved by the FDA for various hematological malignancies and solid tumors since the first ADC, gemtuzumab ozogamicin, was approved in 2000.[17] The combination of ADCs and RDCs plays a complementary role, potentially resulting in a dual killing effect on tumors. Given the high malignancy of GC, we hypothesis combining therapeutic radionuclide ^{131}I and the cytotoxic drug Deruxtecan with an antibody targeting CLDN18.2 to synthesize a radio-antibody-drug conjugate (RADC). The combination of accurate internal irradiation therapy provided by ^{131}I and the cytotoxicity of Deruxtecan can deliver a dual strike against GC.

Materials and Methods

Preparation and Characterization of HLX58-Der

The CLDN18.2 antibody, HLX58, was conjugated to the TopI inhibitor DXd through a maleimide-GGFG peptide linker (MC-GGFG-DXd), hereafter referred to as Deruxtecan (HY-13631E, MedChemExpress). Partial reduction of cysteines forming disulfide bonds between antibody chains was achieved using 1 μg/μL tris (2-carboxyethyl) phosphine (TCEP) in a 50mM potassium phosphate—5mM EDTA solution at pH 6.0 for 1 hour at 37°C with gentle agitation. The molar ratio of HLX58 to TCEP was 1:3. The reducing agent was subsequently removed using a Zeba Spin Desalting Column (7K MWCO; Thermo Fisher Scientific), followed by an immediate reaction of reduced HLX58 with a 10:1 molar excess of Deruxtecan for 4 hours at 37°C. The product, HLX58-Der, was purified using a 0.5 mL ultrafiltration tube (Amicon Ultra, MWCO 30 kDa). The average drug-to-antibody ratio (DAR) for HLX58 conjugates with Deruxtecan was calculated using an AB SCIEX 5600+ quadrupole time-of-flight mass spectrometer (AB SCIEX, Foster City, CA) as described by Yang.[18]

Radiolabeling of HLX58 and HLX58-Der

The CLDN18.2 antibody, HLX58, was labeled with ^{125}I or ^{131}I using the catalyst Iodogen. Briefly, HLX58 (10 μg) and Na[^{125}I]I (185 MBq) or Na[^{131}I]I (185 MBq) were added to an Eppendorf tube containing 20 μg of Iodogen. The mixture was allowed to react at room temperature for 30 minutes. The CLDN18.2-specific ADC, HLX58-Der, was labeled with ^{131}I using a similar method. HLX58-Der (100 μg-1 mg) and Na[^{131}I]I (185 MBq) were added to an Eppendorf tube containing 20 μg of Iodogen and allowed to react for 30 minutes.

The in vitro stability of the labeling products, ^{125}I-HLX58 and ^{131}I-HLX58-Der, was assessed by co-culturing with phosphate-buffered saline (PBS) at a 1:10 dilution (v/v) for 10 and 14 days, respectively. The labeling yield and stability were determined using high performance liquid chromatography (HPLC, Agilent, Canada). Analytical HPLC was performed using a TSKgel SuperSW2000 column (4 μm, 150A, 4.6*300.0 mm). The solvent was a 0.15 M phosphate buffer (PB) solution at pH 6.8. The flow rate was set at 0.35 mL/min.

Cell Lines and Animal Models

The NUGC4 human gastric cancer cell line was generously provided by Henlius Biopharmaceutical Co., Ltd. NUGC4-hCLDN18.2 cells, which stably express human CLDN18.2 protein, were generated by transducing the NUGC4 cell line with a VSV-G pseudotyped lentiviral vector encoding full-length human CLDN18.2. NUGC4 and NUGC4-hCLDN18.2 cells were cultured in Roswell Park Memorial Institute-1640 (RPMI-1640) medium (Basalmedia, Shanghai, China) supplemented with 10% fetal bovine serum (HyClone) at 37 °C in a humidified atmosphere containing 5% CO_2. The cell lines were passaged for less than three months, and the cell stocks were stored in liquid nitrogen.

All animal procedures were conducted in accordance with protocols approved by the Institutional Animal Care and Use Committee of Fudan University. Female Balb/c nude mice (4−6 weeks old, body weight = 20−25 g) were utilized. Subcutaneous tumor models were established by injecting 1×10^6 NUGC4 or NUGC4-hCLDN18.2 cells suspended in 100 μL of phosphate-buffered saline (PBS) subcutaneously into the right shoulder.

Cellular Uptake

For the uptake assays, NUGC4 or NUGC4-hCLDN18.2 cells were seeded into a 24-well plate at a density of 1×10^5 cells per well 24 hours prior to the experiment. The tumor cells were then incubated with ^{125}I-HLX58 or ^{131}I-HLX58-Der (37 kBq per well) at 37 °C for 0.25, 0.5, 0.75, 1.0, 1.5, 2.0, 3.0 and 4.0 hours, respectiveIy. For efflux assays, cells were incubated with ^{125}I-HLX58 or ^{131}I-HLX58-Der (37 kBq per well) for four hours, washed, and subsequently cultured in non-radioactive medium for 0.25, 0.5, 0.75, 1.0, 1.5, 2.0, 3.0 and 4.0 hours, respectiveIy. After incubation, the tumor cells were washed three times with ice-coId PBS and harvested via trypsinization with 0.25% trypsin/0.02% EDTA (HyClone). The cell suspensions were collected and measured using a gamma counter (Nuclear Institute Rihuan Optoelectronic Instrument Co., Ltd, Shanghai, China). The celluIar uptake data were presented as the percentage of the totaI input radioactivity after decay correction.

Cell Binding

In vitro binding affinity and specificity of ^{125}I-HLX58 or ^{131}I-HLX58-Der for CLDN18.2 were assessed using a competitive cell-binding assay. NUGC4-hCLDN18.2 cells were incubated with ^{125}I-HLX-58 or ^{131}I-HLX-58-Der (37 kBq per well) in the presence of ten different concentrations (10^{-13}–10^{-4} M) of unlabeled HLX58 for 120 min. The best-fit 50% inhibitory concentration (IC_{50}) values for NUGC4-hCLDN18.2 cells were calculated by fitting the data with non-linear regression using Graph-Pad Prism 9.0 (Graph-Pad Software, San Diego, CA, USA).

Cell Counting Kit (CCK)-8 Assay

The CCK-8 assay was employed to assess the toxicity of ^{131}I-HLX58-Der to NUGC4-hCLDN18.2 cells. NUGC4-hCLDN18.2 cells were plated onto a 96-well plate (five replicate wells, 1×10^4 cells/well) overnight and then co-cultured with RPMI-1640 medium containing HLX58, HLX58-Der or ^{131}I-HLX58-Der (HLX-58 or HLX-58-Der: 0.1, 1, 10, 100, 1000, 10,000, 100000 ng/mL, ^{131}I: 0.148 MBq) for 48 hours. Subsequently, CCK-8 reagent (10 μL) was added to the cell medium in each well and incubated for 1–2 hours. Finally, a microplate reader was utilized to determine the optical density (OD) at 450 nm. The percentage optical density (OD) for each group relative to that of the control group was calculated.

MicroSPECT/CT Imaging

The mice were utilized for in vivo imaging studies once the tumor volume reached 200–300 mm^3 (approximately 2 weeks after inoculation). NUGC4 or NUGC4-hCLDN18.2 tumor-bearing mice were imaged using a small animal-specific microSPECT/CT scanner (nanoScan@SC SPECT/CT 4 Detector; Mediso Medical Imaging Systems, Budapest, Hungary). Mice were administered potassium iodide (KI) solution (0.05 mg/mL) 2 days prior to microSPECT/CT imaging to minimize the uptake of free iodine by the thyroid tissue. Approximately 7.4 MBq (200 μCi) of ^{125}I-HLX58 or ^{131}I-HLX58-Der (approximately 2 μg of HLX-58) were intravenously injected into each mouse. For the ^{125}I-HLX58 group, static microSPECT images were acquired at 6 h, 1 d, 3 d, 6 d, 10 d, and 14 d post-injection. For the ^{131}I-HLX58-Der group, static microSPECT images were acquired at 6 h, 1 d, 3 d, and 7 d post-injection. In the blocking experiment, each NUGC4-hCLDN18.2 tumor-bearing mouse was scanned following the co-injection of 7.4 MBq of ^{125}I-HLX58 or ^{131}I-HLX58-Der with 5 mg/kg (50-fold) HLX58. Each CT scan (50 kV, 980 μA) lasted 6 minutes and was followed by a microSPECT acquisition lasting 20 to 40 minutes (matrix: 128 × 128, frame time: 30–60 seconds). Upon completion of the acquisition, microSPECT/CT data were reconstructed using TeraTomo 3D (TT3D) dynamic range software. MicroSPECT/CT images were analyzed using Nucline 3.00 (Mediso Medical Imaging Systems). Regions of interest (ROIs) were defined, with contralateral front-limb muscles selected as the background for the microSPECT/CT images. Results were expressed as target-to-nontarget tissue ratios (TNR).

In vitro Autoradiography

To validate the accuracy of microSPECT/CT data regarding the tumor uptake of ^{125}I-HLX58 or ^{131}I-HLX58-Der, tumor tissues were excised for autoradiography. Following imaging, the tumor bearing mice were euthanized to obtain tumor tissues (n = 3 per group). The tumor tissues were dissected in half, fixed in paraformaldehyde for hematoxylin and eosin (H&E) and immunohistochemistry (IHC) staining, or placed on the phosphor screen for 24 hours. Images were captured by scanning the phosphor screen with Typhoon 2.0 (GE Healthcare), and the quantified data were analyzed using ImageQuant TL 8.1 (GE Healthcare). As for immunohistochemistry staining, formalin-fixed paraffin-embedded samples were probed with antibodies against CLDN18.2. After incubation with the primary antibodies, positive cells were visualized using DAB+ as a chromogen.

Pharmacokinetics and Biodistribution

Blood clearance was assessed as one of the pharmacokinetic indicators. Normal BALB/c mice were administered ^{125}I-HLX58 or ^{131}I-HLX58-Der ([^{131}I]: 0.74 MBq; HLX58: 100 μg) via the tail vein (n = 5 per group). At specified time points (1, 10, 30, 60, 120, 240 and 480 min), approximately 10 μL of tail-vein blood was collected using a capillary, weighed, and quantified with a gamma counter for radioactive counting. The measured activity was expressed as the percent injected dose per gram of tissue (%ID/g). Pharmacokinetic parameters were calculated by fitting a nonlinear regression curve using Prism 9.0 (GraphPad, San Diego, CA, USA).

In the biodistribution studies, NUGC4-hCLDN18.2 or NUGC4 xenografts were administered ^{125}I-HLX58 or ^{131}I-HLX58-Der ([^{131}I]: 0.74 MBq; HLX58: 100 μg) via the tail vein (n = 3 per group). The blocking group was initially administered HLX58 to block CLDN18.2. At specified time points (^{125}I-HLX58: 6, 24, 48, 72, 96, 168, 240 and 336 h; ^{131}I-HLX58-Der: 6, 24, 48, 72, 96, 120 and 144 h), tumors as well as selected tissues and organs, were harvested, weighed, and quantified using the gamma counter. The results were reported as the percent injected dose per gram of tissue (%ID/g).

In vivo Treatment

The antitumor efficacy of HLX58-Der was evaluated in NUGC4-hCLDN18.2 tumor models. Mice were randomly assigned to four groups (n = 5 per group) when tumor volumes reached approximately 80 mm^3. Three groups received intravenous injections of HLX58-Der at doses of 2, 5 or 10 mg/kg four times, with interval of 5 days, while the control group was administered PBS. Subsequently, the antitumor efficacy of ^{131}I-HLX58-Der was evaluated. Mice were randomly assigned to five groups (n=5 per group) when tumor volumes reached approximately 80 mm^3. Four groups received intravenous injections of HLX58 (9.80 mg/kg), ^{131}I-HLX58 (HLX58: 9.80 mg/kg, ^{131}I: 3.7 MBq), HLX58-Der (10 mg/kg) or ^{131}I-HLX58-Der (HLX58-Der: 10 mg/kg, ^{131}I: 3.7 MBq) four times with intervals of 5 days, while the control group was administered PBS. All animals were euthanized when the average tumor volume in the control group reached 1000 mm^3. Tumor volumes were measured using the modified ellipsoidal formula V = (length × width^2)/2 each 2 days.

Biosafety

^{131}I-HLX58-Der (HLX58-Der: 10 mg/kg, ^{131}I: 3.7 MBq) was administered to normal mice via the tail vein (n = 5 per group). Vital signs were monitored for 7 consecutive days; thereafter, the mice were euthanized for assessment of routine blood tests, hepatorenal function, and H&E staining of the heart, liver, spleen, lungs, and kidneys.

Statistical Analysis

Graphs were generated using GraphPad Prism software. Data are expressed as mean ± SEM from at least three independent experiments or one representative experiment from three. Statistical analyses were conducted using an unpaired Student's *t*-test. Significance levels of $p<0.05$ were deemed statistically significant.

Results

CLDN18.2-Targeting RADC

The structure of the CLDN18.2-targeting RADC is presented in Figure 1A, consisting of the fully human anti-CLDN18.2 monoclonal antibody HLX58, the therapeutic radioactive isotope ^{131}I, the maleimide GGFG peptide linker, and a derivative of DXd. ^{131}I was labeled on the tyrosine residues of the antibody using the catalyst iodogen. DXd was conjugated to the antibody through the peptide linker. The interchain disulfide bonds were reduced with TCEP HCl to generate cysteine residues for the conjugation of the linker-payload to the antibody. The quadrupole time-of-flight mass spectrometer indicated that the molecular weight of the light chain slightly increased relative to that of the initial antibody. The increase in molecular weight corresponds to that of Deruxtecan, indicating that the DAR of the resulting RADC is approximately 2 (online supplemental Figure S1 and S2). The anti-CLDN18.2 antibody HLX58 labeled with ^{125}I enabled real-time imaging of CLDN18.2 in vivo, which is essential for achieving precise treatment of the RADC.

The purities of HLX58 and HLX58-Der were assessed using HPLC. As showed in Figure 1B, the retention time of HLX58-Der was approximately 7.22 minutes, which is similar to that of HLX58 (7.0 minutes). The stability of ^{131}I-HLX58-Der was confirmed by radio-HPLC (Figure 1C, D and online supplemental Figure S3). ^{131}I-HLX58-Der remained stable for up to 10 days at 4°C. The chemical purity of ^{131}I-HLX58-Der decreased from 97.60 ± 0.82% on day 0 to 82.43 ± 2.40% on day 10. The radiolabeling efficiency of ^{131}I for HLX58-Der was 82.03 ± 1.96% on day 10. The radiochemical purity of ^{125}I-HLX58, as determined by radio-HPLC, indicated that the radiolabeling efficiency of ^{125}I for HLX58 was 87.80 ± 0.45% on day 14 (Figure 1E, F and online supplemental Figure S4).

Cell Binding of the RADC

^{125}I-labeled HLX58, an antibody targeting CLDN18.2, is applicable for real-time imaging of CLDN18.2 in tumor tissues using microSPECT/CT imaging. This serves as a prerequisite for ^{131}I-HLX58-Der in the precise treatment of tumors. Consequently, we investigated the uptake and efflux of ^{125}I-HLX58 in CLDN18.2-positive NUGC4-hCLDN18.2 and CLDN18.2-negative NUGC4 WT tumor cells. The cell uptake studies revealed that ^{125}I-HLX58 bound specifically to NUGC4-hCLDN18.2 cells and not to NUGC4 WT cells. During the initial hour of incubation, the uptake of ^{125}I-HLX58 by NUGC4-hCLDN18.2 cells was approximately 2.01% ± 0.19. After 4 hours of incubation, the maximum uptake rate of ^{125}I-HLX-58 by NUGC4-hCLDN18.2 cells reached 5.50% ± 0.80. Cell efflux studies indicated that ^{125}I-HLX58 was retained in NUGC4-hCLDN18.2 cells. Over a 4-hour period, approximately 4.30% ^{125}I-HLX58 efflux (from a total of 6.51% to 2.21%) occurred in NUGC4-hCLDN18.2 cells (Figure 2A and B). The cellular uptake and retention results for ^{125}I-HLX58 in CLDN18.2-negative NUGC4 WT tumor cells after 2 hours of incubation were significantly lower. The uptake rate of ^{125}I-HLX58 was consistently low at 0.59% ± 0.20, significantly lower than that in NUGC4-hCLDN18.2 cells ($p < 0.05$; Figure 2A and B).

A cell-based competitive assay was employed to assess the binding affinity and specificity of ^{125}I-HLX58 to CLDN18.2 expressed on NUGC4-hCLDN18.2 tumor cells. ^{125}I-HLX58 served as a CLDN18.2-specific radioligand for competitive displacement, with HLX58 concentrations ranging from 10^{-12} to 10^{-4} M. The IC_{50} value is defined as the concentration of HLX58 required to displace 50% of the bound ^{125}I-HLX58 from NUGC4-CLDN18.2 tumor cells. The IC_{50} value for HLX58 was determined to be 2.98 nM (Figure 2C).

To confirm the target specificity of ^{131}I-HLX58-Der, we evaluated its binding activity against CLDN18.2-positive NUGC4-hCLDN18.2 and CLDN18.2-negative NUGC4 WT tumor cells, in addition to assessing cell growth inhibition activity. The uptake of ^{131}I-HLX58-Der in NUGC4-hCLDN18.2 cells was measured to be 4.35% ± 0.51 during the initial 2 hours of incubation. After 4 hours of incubation, the uptake of ^{131}I-HLX58-Der in NUGC4-hCLDN18.2 cells significantly increased to 5.95% ± 0.39 of the total input radioactivity (Figure 2D). In CLDN18.2-negative NUGC4 WT cells, the cellular uptake of ^{131}I-HLX58-Der was minimal regarding the total input radioactivity after 4 h of incubation. The uptake value was determined to be 0.67% ± 0.27 for the NUGC4 WT cells, significantly lower than that for NUGC4-CLDN18.2 cells (5.95% ± 0.39 and $p < 0.05$). The cellular uptake study revealed that ^{131}I-HLX58-Der strongly binds to NUGC4-hCLDN18.2 cells but minimally to NUGC4 WT cells. The efflux study demonstrated that ^{131}I-HLX58-Der exhibited low cellular efflux rates after 4 hours in NUGC4-hCLDN18.2 cells (Figure 2E). The competitive

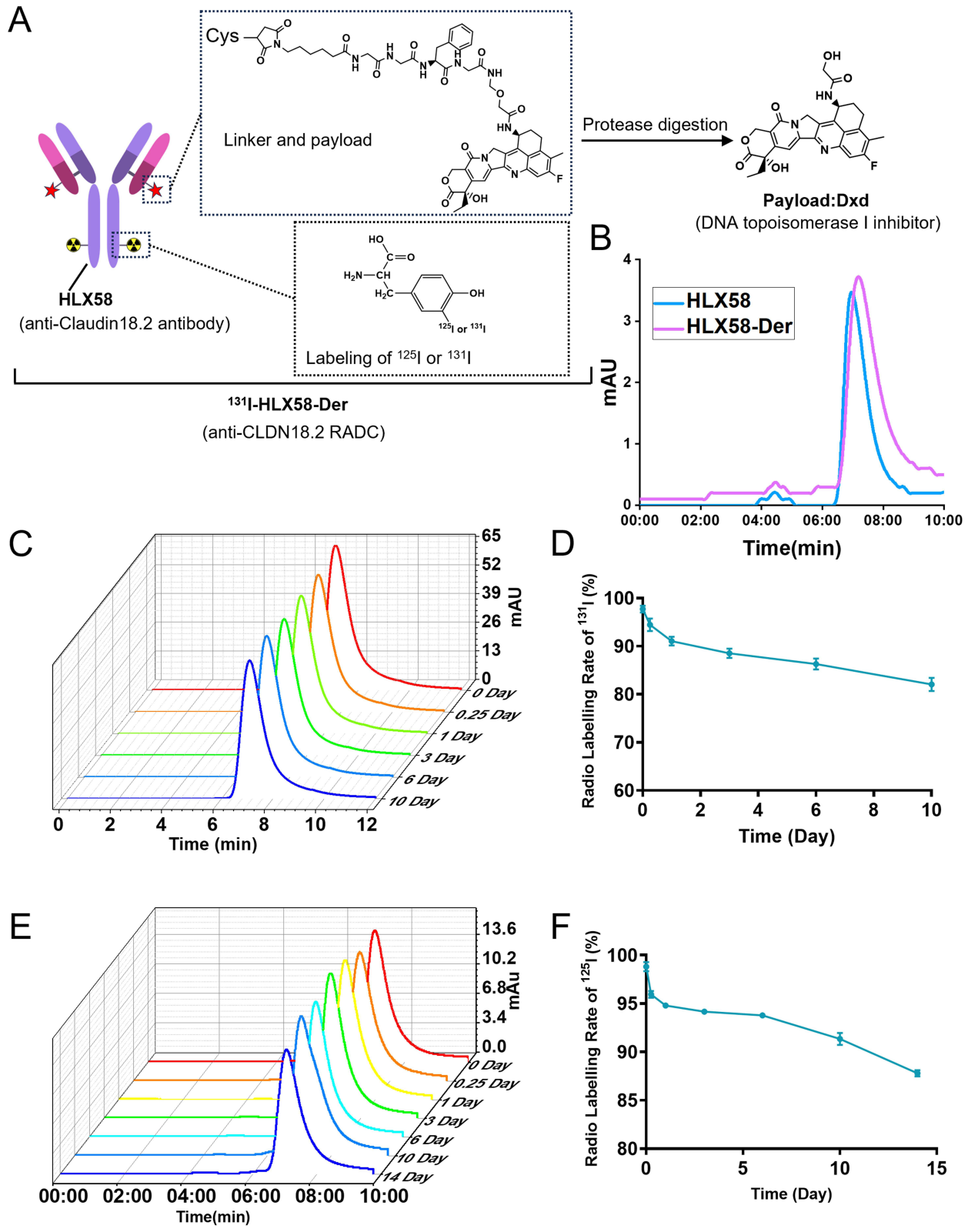

Figure 1 The synthesis of radio-antibody-drug conjugate. (**A**) Schematic representation of the structure of ^{125}I-HLX58 and ^{131}I-HLX58-Der. DXd was conjugated to HLX58 through a maleimide-GGFG peptide linker. (**B**) Representative HPLC spectrum of HLX58 and HLX58-Der. (**C** and **D**) Stability of ^{131}I-HLX58-Der incubated in saline at 4°C for 10 days in vitro. (**E** and **F**) Stability of ^{125}I-HLX58 incubated in saline at 4°C for 14 days in vitro.

https://doi.org/10.2147/IJN.S501689

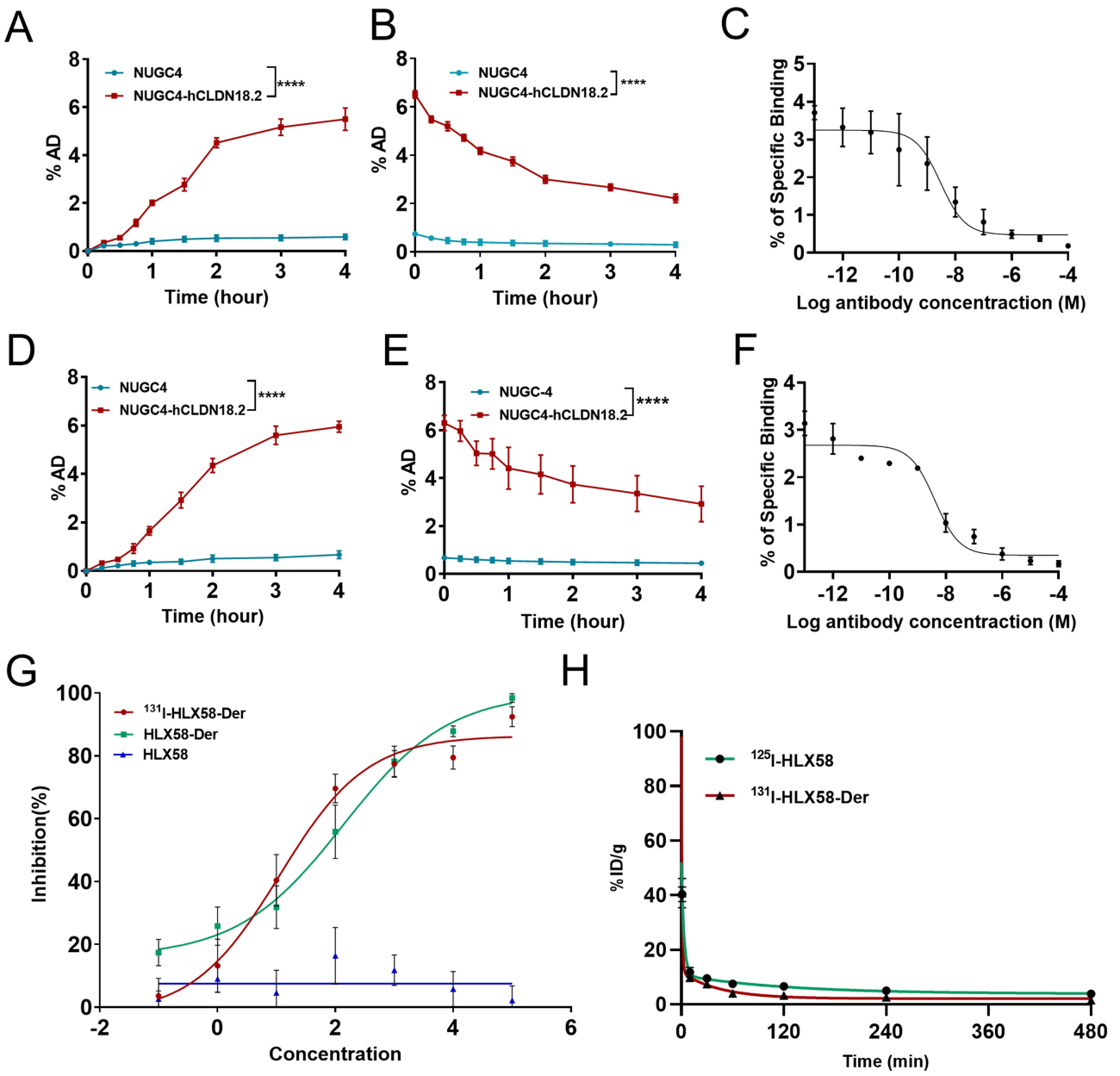

Figure 2 The targeting of ^{125}I-HLX58/^{131}I-HLX58-Der to CLDN18.2. (**A**) Cellular uptake assays of ^{125}I-HLX58 in NUGC4 and NUGC4-hCLDN18.2 tumor cells. %AD = percentage administered dose. Data were expressed as mean ± SEM (**** P<0.0001). (**B**) Cellular efflux assays of ^{125}I-HLX58 in NUGC4 and NUGC4-hCLDN18.2 tumor cells. %AD = percentage administered dose. Data were expressed as mean ± SEM (**** P<0.0001). (**C**) Competitive binding curves for half-maximal inhibitory concentration determination of ^{125}I-HLX58 in NUGC4-hCLDN18.2 tumor cells, using HLX58 as competitive inhibitor. (**D**) Uptake of ^{131}I-HLX58-Der in NUGC4 and NUGC4-hCLDN18.2 tumor cells. %AD = percentage administered dose. Data were expressed as mean ± SEM (**** P<0.0001). (**E**) Retention curves of ^{131}I-HLX58-Der in NUGC4 and NUGC4-hCLDN18.2 tumor cells. %AD = percentage administered dose. Data were expressed as mean ± SEM (**** P<0.0001). (**F**) Competitive binding curves for half-maximal inhibitory concentration determination of ^{131}I-HLX58-Der in NUGC4-hCLDN18.2 tumor cells, using HLX58 as competitive inhibitor. (**G**) ^{131}I-HLX58-Der showed significant higher cytotoxicity towards NUGC4-hCLDN18.2 cells than HLX58-Der and HLX-58. IC_{50} denotes half maximal inhibitory concentration. (**H**) Blood radioactivity profile of ^{125}I-HLX58 and ^{131}I-HLX58-Der. Data were expressed as mean ± SEM.

cell binding experiment involving NUGC4-hCLDN18.2 cells and HLX58 demonstrated strong inhibition of CLDN18.2 in the nanomole range. The IC_{50} value for HLX58 was determined to be 4.12 nM (Figure 2F).

Cytotoxic Effects and Pharmacokinetics of the RADC

RADC binds to CLDN18.2 through the antibody-HLX58. Lysosomal enzymes, which are highly expressed in tumor cells, can decompose the tetrapeptide and release DXd.[19] ^{131}I and DXd synergistically induce cell death in tumors. We

therefore evaluated the cytotoxic activity of ^{131}I-HLX58-Der using CLDN18.2-positive NUGC4-hCLDN 18.2 cells (Figure 2G). NUGC4-hCLDN18.2 cells were susceptible to ^{131}I-HLX58-Der, with an IC_{50} of 11.28 ng/mL. Conversely, the cytotoxic activity of HLX58-Der markedly decreased in NUGC4-hCLDN18.2 cells, with an IC_{50} of 136.6 ng/mL. HLX58 exhibited no significant cytotoxic effect on NUGC4-hCLDN18.2 cells. These results indicate that ^{131}I significantly enhances the cytotoxic effect of HLX58-Der, an ADC targeting CLDN18.2, on tumor cells. Under the combined effects of ^{131}I and DXd, RADC demonstrated a significant inhibitory effect on CLDN18.2-positive tumor cells.

To investigate the pharmacokinetic parameters of ^{125}I-HLX58 and ^{131}I-HLX58-Der, blood clearance was assessed in normal mice (Figure 2H). The distribution-phase half-life ($t_{1/2\alpha}$) values for ^{125}I-HLX58 and ^{131}I-HLX58-Der were between approximately 0–2 min (^{125}I-HLX58, 2.11 min; ^{131}I-HLX58-Der, 0.64 min). The clear-phase half-life ($t_{1/2\beta}$) values of ^{125}I-HLX58 and ^{131}I-HLX58-Der were between approximately 30–80 min (^{125}I-HLX58, 84.20 min; ^{131}I-HLX58-Der, 31.35 min).

Precise SPECT/CT Imaging of ^{125}I-HLX58 for CLDN18.2

The cell uptake and efflux assays demonstrated that a significant quantity of ^{125}I-HLX58 was retained within cells, prompting an investigation into its tumor-targeting efficacy and biodistribution.

Static microSPECT/CT scans were conducted at various time points over 14 days following the administration of ^{125}I-HLX58 to nude mice bearing human gastric cancer NUGC4-hCLDN18.2 and NUGC4-WT xenografts (n=5/group). The CLDN18.2-positive NUGC4-hCLDN18.2 tumors were clearly visible and exhibited a favorable tumor-to-background contrast at all time points, whereas the CLDN18.2-negative NUGC4-WT tumors displayed minimal uptake of ^{125}I-HLX58. Representative images depicting tumors at 6 h, 1, 3, 6, 10, and 14 d pi were shown in Figure 3A. The maximum tumor-to-normal tissue (T/NT) ratio of ^{125}I-HLX58 was approximately 16.76 ± 6.30 at 6 d pi (Figure 3B).

Blocking experiments were conducted to evaluate the specificity of ^{125}I-HLX58 for CLDN18.2. Tumor uptake of radiolabeled ^{125}I-HLX58 was significantly reduced following co-injection with non-radiolabeled HLX58 (5 mg/kg of mouse body weight). A representative decay-corrected microSPECT/CT image of CLDN18.2-positive NUGC4-hCLDN18.2 xenograft at 3 d pi (^{125}I-HLX58 plus HLX58) is presented in Figure 3C. When non-radiolabeled HLX58 was co-injected, the T/NT ratio was 2.89 ± 0.89 at 3 d pi (Figure 3D). Tumors that were not blocked with non-radiolabeled HLX58 showed significantly higher uptake (13.70 ± 1.66; $P < 0.05$). Additionally, the T/NT ratio of the CLDN18.2-negative NUGC4-WT tumors was 2.25 ± 0.43 at 3 d pi. Thus, the results from the blocking studies confirm that ^{125}I-HLX58 can be utilized for precise imaging of CLDN18.2 in tumors.

Images from in vitro autoradiography further confirmed that the accumulation of ^{125}I-HLX58 in NUGC4-hCLDN18.2 tumor tissues was significantly higher than that in both NUGC4-hCLDN18.2 blocked and NUGC4-WT tumor tissues (Figure 3E). Immunohistochemistry staining of the tumor tissues revealed a high expression level of CLDN18.2 in the NUGC4-hCLDN18.2 xenograft. As anticipated, CLDN18.2 expression was not observed in NUGC4-WT tumor tissues (Figure 3E).

Long-term biodistribution studies of ^{125}I-HLX58 conducted up to 336 h post-injection in NUGC4-hCLDN18.2 tumor–bearing mice facilitated dosimetry calculations. ^{125}I-HLX58 exhibited substantial tumor retention (2.59 ± 0.17%ID/g at 6 h and 5.73 ± 0.35%ID/g at 48 h) and rapid clearance from the liver (1.84 ± 0.10%ID/g at 6 h and 1.12 ± 0.12%ID/g at 24 h; Figure 3F and online supplemental Table 1) and kidneys (1.15 ± 0.19%ID/g at 6 h and 1.34 ± 0.04%ID/g at 24 h; Figure 3F and online supplemental Table 1). The retention of ^{125}I-HLX58 in NUGC4-hCLDN18.2 blocked (0.54 ± 0.21%ID/g at 48 h) and NUGC4-WT (0.54 ± 0.14%ID/g at 48 h) tumor tissues was significantly lower than that in NUGC4-hCLDN18.2 tumor tissues (online supplemental Figure S5). Collectively, these findings demonstrate that the biodistribution of ^{125}I-HLX58 correlates with the expression of CLDN18.2 in tumor tissues. ^{125}I-HLX58 demonstrated significant targeting of CLDN18.2.

MicroSPECT/CT Imaging for the Monitoring of the Biodistribution of RADC

One of the major advantages of RADC in cancer treatment is the ability to monitor its real-time distribution in vivo with the aid of radioisotope and imaging technologies. Following RADC injection, the distribution of RADC was monitored in vivo for up to 7 days post-injection of ^{131}I-HLX58-Der using SPECT/CT imaging.

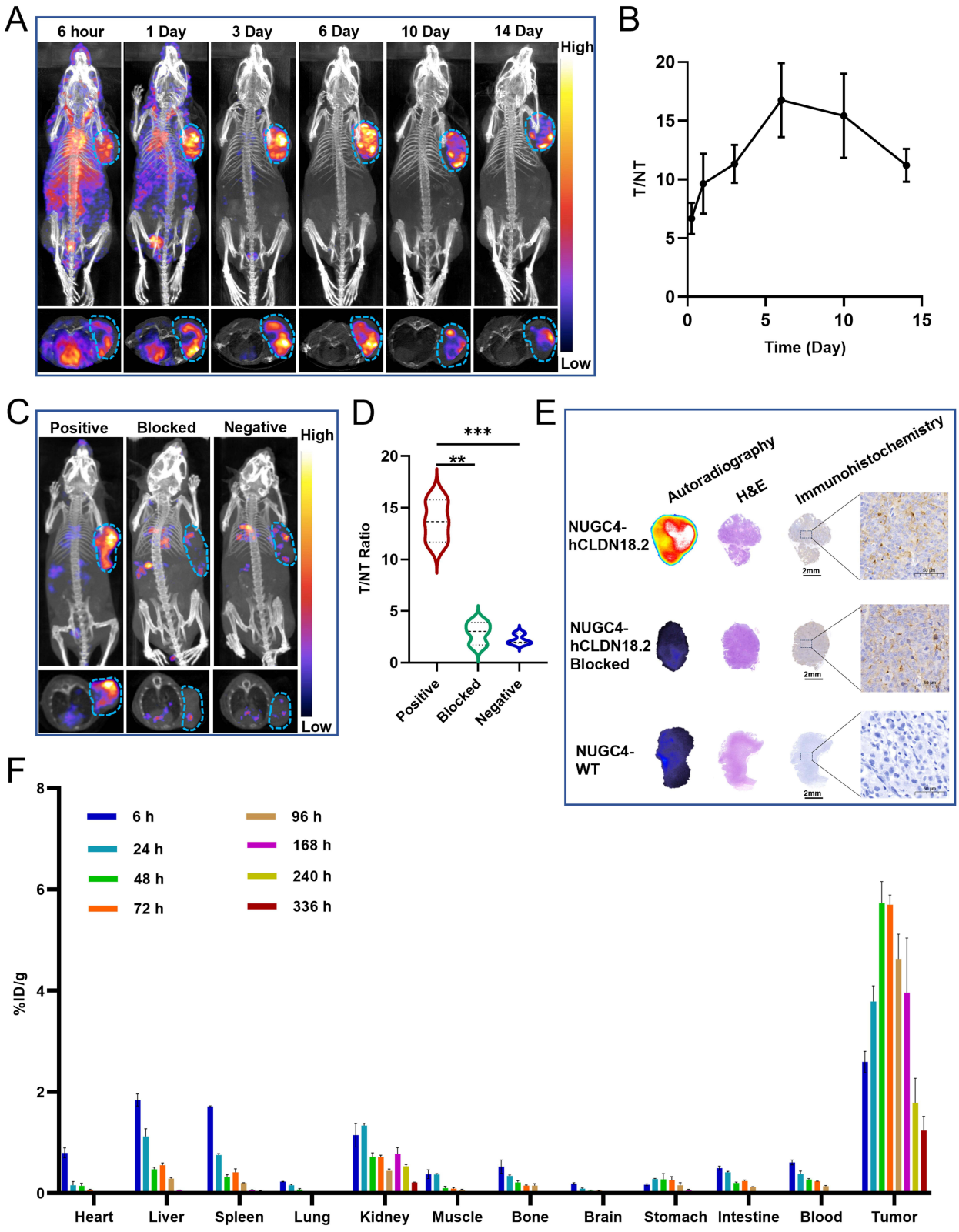

Figure 3 ^{125}I-HLX58 for the microSPECT/CT imaging targeting CLDN18.2. (**A**) Representative ^{125}I-HLX58 microSPECT/CT images of mice bearing NUGC4-hCLDN18.2 tumors. 7.4 MBq ^{125}I-HLX58 was injected via tail vein for each mouse. (**B**) The ratios of tumor-to-nontarget tissue derived from ^{125}I-HLX58 microSPECT/CT images in NUGC4-hCLDN18.2 tumor models (n = 5). (**C**) Representative ^{125}I-HLX58 microSPECT/CT images of NUGC4-hCLDN18.2 (non-blocked and blocked with HLX58) and NUGC4 tumors xenografts. (**D**) Tumor-to-nontarget tissue ratios derived from ^{125}I-HLX58 microSPECT/CT images in NUGC4-hCLDN18.2 (non-blocked and blocked) and NUGC4 tumor models (n = 3, ** P=0.0013, *** P=0.0007). (**E**) Representative images of the autoradiography and corresponding H&E and IHC staining of NUGC4-hCLDN18.2 (non-blocked and blocked) and NUGC4 tumors. (**F**) Biodistribution of ^{125}I-HLX58 in NUGC4-hCLDN18.2 models.

https://doi.org/10.2147/IJN.S501689

Systemic microSPECT/CT imaging was employed to continuously monitor nude mice bearing human gastric cancer NUGC4-hCLDN18.2 and NUGC4-WT xenografts (n=5/group) for 7 days following the administration of ^{131}I-HLX58-Der. ^{131}I-HLX58-Der demonstrated significant accumulation in CLDN18.2-positive NUGC4-hCLDN18.2 tumors. However, accumulation significantly decreased in CLDN18.2-negative NUGC4-WT tumors. Representative images of tumors at 6 h, 1, 3 and 7 d pi are presented in Figure 4A and B. The maximum T/NT ratio of ^{131}I-HLX58-Der were approximately 12.13 ± 3.87 at 7 d pi. The specificity of ^{131}I-HLX58-Der for CLDN18.2 was confirmed through blocking experiments. The accumulation of ^{131}I-HLX58-Der was significantly reduced following co-injection with non-radiolabeled HLX58 (5 mg/kg of mouse body weight). Additionally, the accumulation of ^{131}I-HLX58-Der was low in CLDN18.2-negative NUGC4-WT xenografts (Figure 4C). The T/NT ratio of the CLDN18.2-positive NUGC4-hCLDN18.2 tumors was 11.30 ± 2.33, which was higher than that of the blocking group (1.73 ± 0.45, $p<0.05$) and the CLDN18.2-negative group (1.74 ± 0.19, $p<0.05$) (Figure 4D).

In vitro autoradiography and H&E/IHC staining further confirmed that the accumulation of ^{131}I-HLX58-Der in tumor tissues was positively correlated with CLDN18.2 expression (Figure 4E). Long-term biodistribution studies of ^{131}I-HLX58-Der conducted up to 144 h post-injection in NUGC4-hCLDN18.2 tumor–bearing mice facilitated dosimetry calculations. The tumor retention of ^{131}I-HLX58-Der was 2.77 ± 0.24%ID/g at 6 h and 5.83 ± 0.41%ID/g at 72 h. ^{131}I-HLX58-Der was primarily excreted via the liver (1.09 ± 0.19%ID/g at 24 h and 0.39 ± 0.07%ID/g at 72 h; Figure 4F and online supplemental Table 2) and kidneys (0.92 ± 0.07%ID/g at 24 h and 0.56 ± 0.02%ID/g at 72 h; Figure 4F and online supplemental Table 2). The retention of ^{131}I-HLX58-Der in NUGC4-hCLDN18.2 tumor tissues (5.63 ± 1.66%ID/g at 72 h) was significantly higher than that in NUGC4-hCLDN18.2-blocked tumor tissues (0.49 ± 0.19%ID/g at 72 h, $p<0.05$) and NUGC4-WT tumor tissues (0.31 ± 0.12%ID/g at 72 h, $p<0.05$) (online supplemental Figure S6). Collectively, these findings confirm that ^{131}I-HLX58-Der demonstrates significant specificity for CLDN18.2.

Therapeutic Efficacy and Toxicity Assessment of RADC

To assess the antitumor activity of HLX58-Der in vivo, we utilized a human gastric cancer cell line, NUGC4-hCLDN18.2, in xenograft models. 20 mice bearing NUGC4-hCLDN18.2 tumors were randomly assigned to 4 groups and administered escalating doses of HLX58-Der at 2, 5, and 10 mg/kg intravenously (Figure 5A). Treatment with HLX58-Der at 5 and 10 mg/kg significantly inhibited tumor growth compared to the control group at 22 days post-administration ($p < 0.05$; Figure 5B–D and online supplemental Figure S7). To confirm the synergistic inhibitory effects of ^{131}I and DXd in ^{131}I-HLX58-Der, 25 mice bearing NUGC4-hCLDN18.2 xenografts were divided into five groups and received vehicle control, HLX58, ^{131}I-HLX58, HLX58-Der, or ^{131}I-HLX58-Der treatment (Figure 5A). Compared to the control, ^{131}I-HLX58 and HLX58-Der groups, ^{131}I-HLX58-Der further inhibited the growth of tumors ($p < 0.05$; Figure 5E–G and online supplemental Figure S8).

After the intervention with ^{131}I-HLX58-Der on day 22, no abnormalities were observed in H&E sections of the heart, liver, spleen, lung and kidney compared to the control group (Figure 6A). Additionally, the results of hepatorenal function and blood routine tests indicated no evidence of systemic biological toxicity following ^{131}I-HLX58-Der therapy (Figure 6B and C).

Discussion

ADCs exemplify molecularly-targeted chemotherapies, utilizing a molecule designed against a specific target (such as a monoclonal antibody) to deliver a cytotoxic agent linked chemically to a specific tumor-associated protein or antigen.[19,20] ADCs selectively deliver cytotoxic agents to tumor cells while potentially sparing normal tissues, thereby reducing off-target side-effects.[21] Several ADCs have been approved worldwide, and many others are currently in clinical trials. The payloads of these ADCs include auristatins, camptothecins, maytansinoids, pyrrolobenzodiazepines, duocarmycins and halichondrins, which belong to classes of microtubule polymerization inhibitors (such as auristatins and maytansines) and topoisomerase I inhibitors (such as camptothecin).[22] DS-8201a, a HER2-targeting ADC, consists of an anti-HER2 antibody and a derivative of DXd, which is a topoisomerase I inhibitor.[23] DXd, acting as antiproliferation agent, can induce cell cycle arrest specifically in the G2/M phase. Cells in this phase are recognized to be more sensitive to radiation.[16,24] Since its discovery, CLDN18.2 has garnered significant attention, with the clinical success of Zolbetuximab demonstrating the developmental potential of this

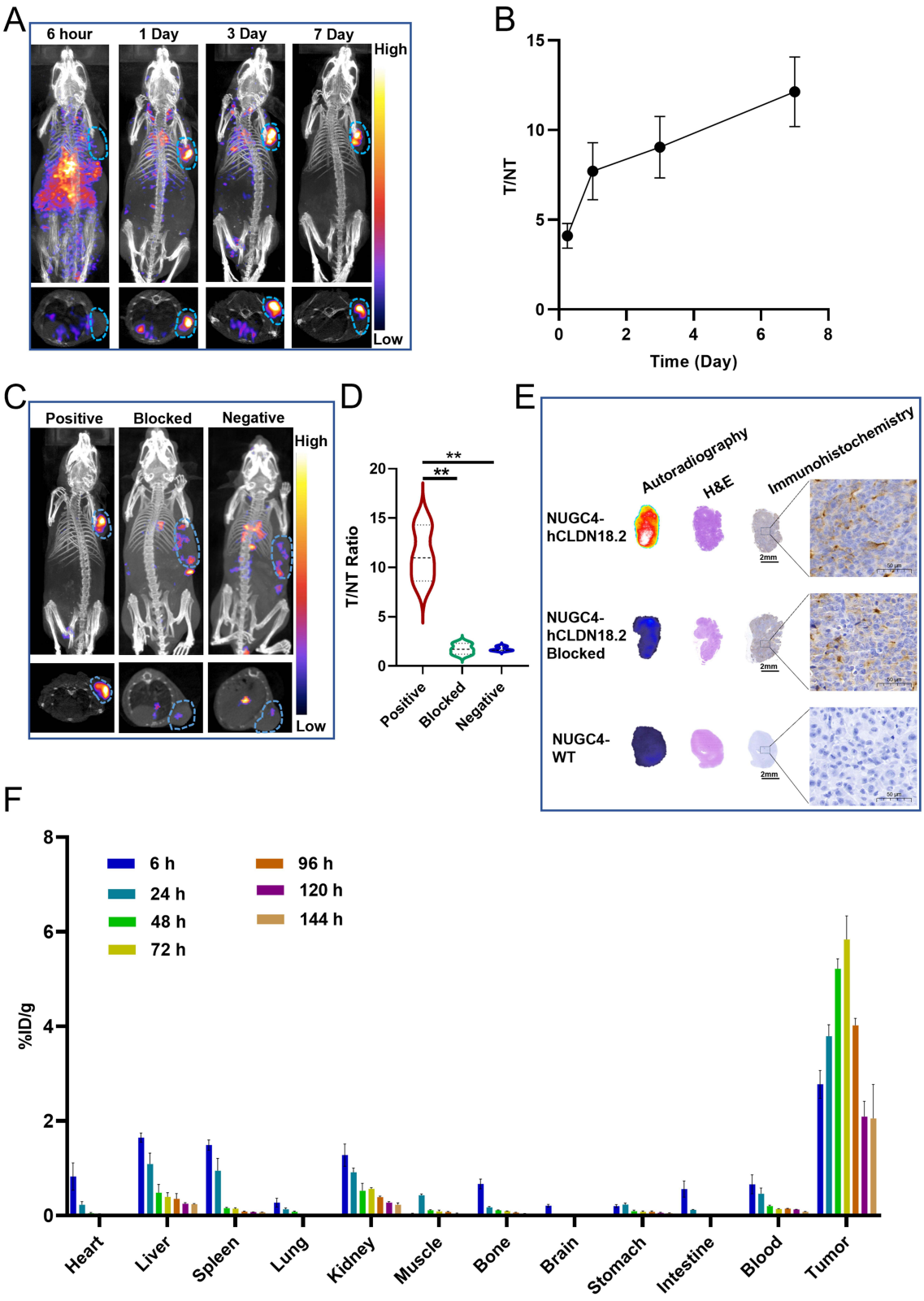

Figure 4 MicroSPECT/CT imaging for the monitoring of the biodistribution of RADC. (**A**) Representative ^{131}I-HLX58-Der microSPECT/CT images of mice bearing NUGC4-hCLDN18.2 tumors. 7.4 MBq ^{131}I-HLX58-Der was injected via tail vein for each mouse. (**B**) The ratios of tumor-to-nontarget tissue derived from ^{131}I-HLX58-Der microSPECT/CT images in NUGC4-hCLDN18.2 tumor models (n = 5). (**C**) Representative ^{131}I-HLX58-Der microSPECT/CT images of NUGC4-hCLDN18.2 (non-blocked and blocked with HLX58) and NUGC4 tumors xenografts. (**D**) Tumor-to-nontarget tissue ratios derived from ^{131}I-HLX58-Der microSPECT/CT images in NUGC4-hCLDN18.2 (non-blocked and blocked) and NUGC4 tumor models (n = 3, ** P<0.005). (**E**) Representative images of the autoradiography and corresponding H&E and IHC staining of NUGC4-hCLDN18.2 (non-blocked and blocked) and NUGC4 tumors. (**F**) Biodistribution of ^{131}I-HLX58-Der in NUGC4-hCLDN18.2 models (n=3).

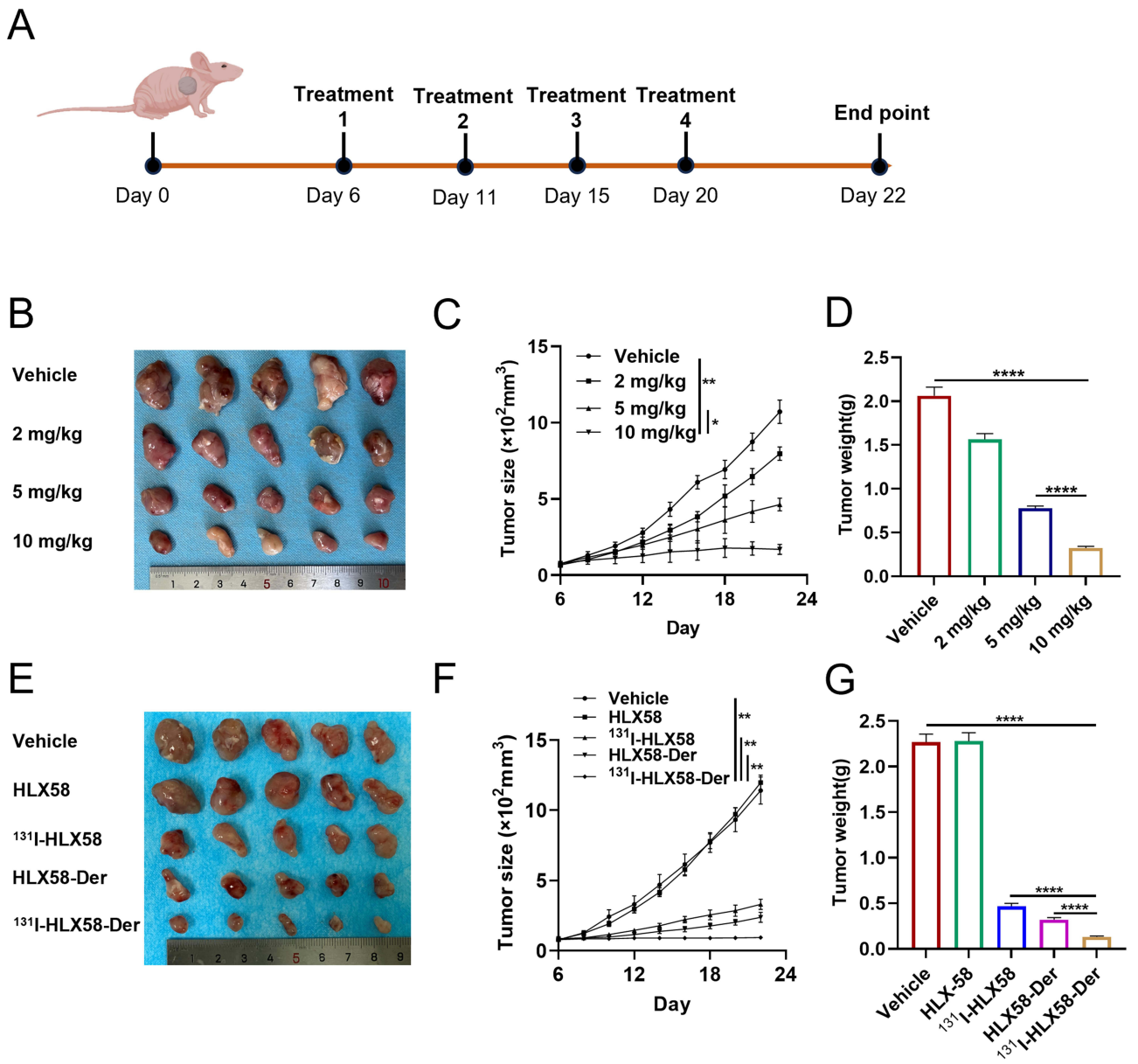

Figure 5 Therapeutic efficacy of ^{131}I-HLX58-Der. (**A**) Diagram of experimental design for the treatment of mice bearing NUGC4-hCLDN18.2 tumors. (**B**) Photographs of tumors from NUGC4-hCLDN18.2 xenografts after treatments with vehicle or HLX58-Der (2 mg/kg, 5 mg/kg and 10 mg/kg) (n = 5). (**C**) Growth curve of NUGC4-hCLDN18.2 tumors after HLX58-Der or vehicle treatment. Vehicle (PBS), HLX58-Der (2 mg/kg, 5 mg/kg and 10 mg/kg) (* P=0.0196, ** P=0.0095). (**D**) Tumor weight of NUGC4-hCLDN18.2 tumors after HLX58-Der or vehicle treatment. Vehicle (PBS), HLX58-Der (2 mg/kg, 5 mg/kg and 10 mg/kg). Data were presented as Mean ± SEM (**** P<0.0001). (**E**) Photographs of tumors from NUGC4-hCLDN18.2 xenografts after treatments with ^{131}I-HLX58-Der, HLX58-Der, ^{131}I-HLX58, HLX58 or vehicle (n = 5). (**F**) Growth curve of NUGC4-hCLDN18.2 tumors after ^{131}I-HLX58-Der, HLX58-Der, ^{131}I-HLX58, HLX58 or vehicle treatment (** P<0.0028). (**G**) Tumor weight of NUGC4-hCLDN18.2 tumors after ^{131}I-HLX58-Der, HLX58-Der, ^{131}I-HLX58, HLX58 or vehicle treatment. Data were presented as Mean ± SEM (**** P<0.0001).

target.[25,26] In this context, an increasing number of ADCs targeting CLDN18.2 have been developed (ClinicalTrial. gov). Although numerous clinical trials for mAb-based CLDN18.2 therapy have been completed or are currently ongoing, no regulatory approvals have been granted due to limited clinical benefits in these trials. Recent research indicates that the ADC drug EO-3021, targeting CLDN18.2, did not meet expectations (Elevation Oncology), and its limitations present opportunities for other competitors to excel.

Radiotheranostics represent a relevant strategy for several cancers.[27,28] This approach utilizes the same targeting ligand, combining molecular imaging with targeted radionuclide therapy (TRT). Molecular imaging allows for monitoring of the target at diseased sites, while cytotoxic radiation delivered to these areas inhibits tumor growth.[29] Cytotoxic

https://doi.org/10.2147/IJN.S501689

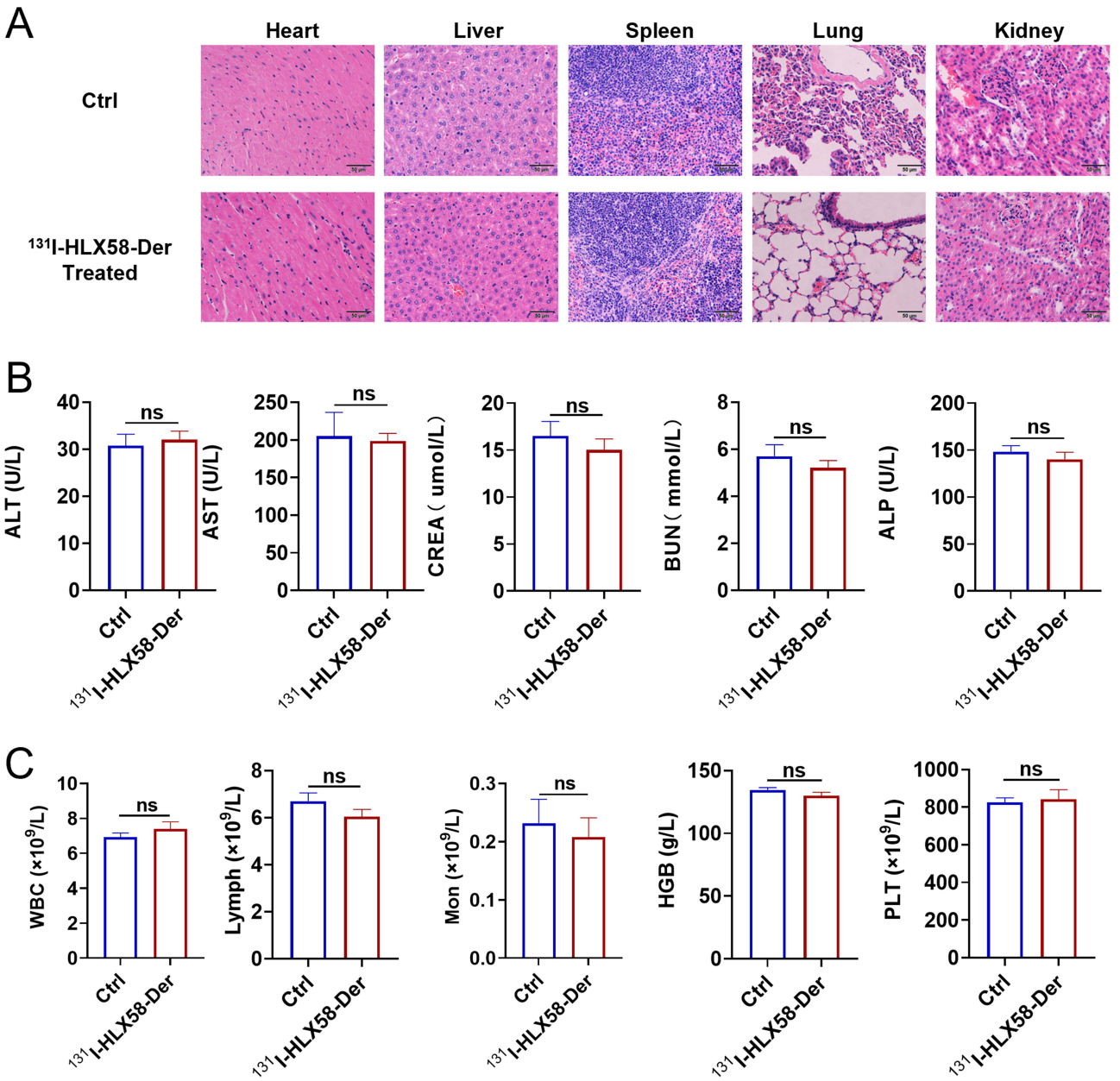

Figure 6 Toxicity assessment of ^{131}I-HLX58-Der. (**A**) H&E staining on major organ tissues of control and experiment groups for in vivo toxicity evaluation after intravenous injection of saline or ^{131}I-HLX58-Der. Scale bar = 50 μm. (**B**) Hepatorenal function analysis of control and experiment groups for in vivo toxicity evaluation after intravenous injection of saline or ^{131}I-HLX58-Der. Data are presented as mean ± SEM (n = 3, ns means the statistical difference is not significant). (**C**) Routing blood analysis of control and experiment groups for in vivo toxicity evaluation after intravenous injection of saline or ^{131}I-HLX58-Der. Data are presented as mean ± SEM (n = 3, ns means the statistical difference is not significant).

radiation can involve α-emitting, β-emitting, or Auger electron–emitting radionuclides. Various targeting ligands, particularly monoclonal antibodies, have been extensively explored.[30,31] Over the past few years, there has been exponential growth in the development and acceptance of radiotheranostics in oncology, with successful applications of ^{131}I in treating thyroid cancer indicating a promising future for this field. Monoclonal antibodies are particularly appealing as targeting ligands due to their high binding affinity, specificity, and ability to distribute homogeneously within target tissues.[32,33] Leveraging the radiosensitizing properties of DXd and the internal radiation capabilities of ^{131}I, we explored a novel paradigm that combines DXd, which facilitates radiosensitization, with ^{131}I for internal radiation therapy in tumor treatment. In this study, we engineered a new CLDN18.2-targeting RADC, ^{131}I-HLX58-Der, demonstrating its CLDN18.2-specific action and payload-derived antitumor activity in preclinical cancer models. By targeting

CLDN18.2, this mAb-based radiopharmaceutical presents a promising avenue for therapeutic interventions in various cancers.

The efficacy of treatment with RADCs or ADCs hinges on the adequate expression of specific targets at diseased sites, facilitating the effective accumulation of drugs and radioactive isotopes within the lesions, ultimately leading to tumor eradication. Traditional methods for detecting targets involve pathological biopsy; however, this approach has limitations that prevent a comprehensive and real-time evaluation of lesion targets. In contrast, molecular imaging offers the capability to monitor target expression in real time, thereby providing a foundation for personalized treatment strategies for patients receiving RADCs. Consequently, molecular imaging targeting CLDN18.2 serves as a critical reference point for assessing the potential of RADCs to effectively inhibit tumor growth.

HLX58-Der was analyzed using a quadrupole time-of-flight mass spectrometer, which revealed a predominant DAR of 2 (Figure 1A). As previously reported, the "half-antibody" formed by intrachain bridging of the heavy chain cysteines in the hinge region with a single linker-drugs (+1) was identified as the primary product (online supplemental Figure S1 and S2). HLX58-Der was labeled with ^{131}I to produce RADC-^{131}I-HLX58-Der. HLX58 labeled with ^{125}I can be utilized for precise imaging of CLDN18.2 in tumor xenografts. The stabilities of ^{131}I-HLX58-Der and ^{125}I-HLX58 were assessed over 10 and 14 days, respectively. The results of the cell uptake and efflux studies confirmed that ^{125}I-HLX58 and ^{131}I-HLX58-Der were taken up and retained in CLDN18.2 positive NUGC4-hCLDN18.2 cells (Figure 2A, B, D and E). Additionally, the competitive binding assays demonstrated the binding affinity and specificity of ^{125}I-HLX58 and ^{131}I-HLX58-Der for CLDN18.2 on NUGC4-hCLDN18.2 cells (Figure 2C and F). The in vitro IC_{50} value of HLX58-Der was 136.60 ng/mL, indicating its cytotoxicity toward NUGC4-hCLDN18.2 cells. Furthermore, the cytotoxicity of ^{131}I-HLX58-Der against NUGC4-hCLDN18.2 cells was significantly greater than that of HLX58-Der, as evidenced by the IC_{50} values (IC_{50}=11.28 ng/mL, $p<0.05$) (Figure 2G). The half-lives ($t_{1/2}$) of ^{125}I-HLX58 and ^{131}I-HLX58-Der, as indicated by the blood clearance assay, were sufficiently short to mitigate damage to major organs.

We have successfully demonstrated specific detection of CLDN18.2-positive tumors in mice using ^{125}I-HLX58. A higher and more specific accumulation in CLDN18.2-positive tumors was observed, while retention in other tissues remained low. The results of the biodistribution studies align with the imaging findings. ^{125}I-HLX58 was rapidly cleared from the liver and kidneys, whereas retention in the CLDN18.2-positive tumor was sustained (Figure 3F). For therapeutic purposes, we selected the β-emitting radionuclide, ^{131}I. Imaging and long-term biodistribution studies revealed high and sustained tumor accumulation of ^{131}I-HLX58-Der in NUGC4-hCLDN18.2 tumors following systemic administration (Figure 4). The long-term toxicity of repeated administration of therapeutic ^{131}I-HLX58-Der was further evaluated. Mice in all treatment groups survived until the conclusion of the study without any instances of weight loss (online supplemental Figure S7 and S8). Histopathologic analysis revealed no cellular changes in the major organs following the administration of ^{131}I-HLX58-Der compared to the control group.

In summary, our findings underscore the therapeutic potential of the RADC format. As the first RADC, ^{131}I-HLX58-Der combines therapeutic radioactive isotope with cytotoxic drug for anti-tumor therapy, which is an innovative point in the field of nuclear medicine. Although promising, the versatility of this molecular format requires further assessment regarding other combinations of mAbs, radioisotopes, and payloads. In particular, α-emitting radionuclides, such as ^{177}Lu, ^{223}Ra, and ^{225}Ac, appear to offer significant advantages in tumor treatment. However, due to the limitations associated with the radiolabeling of antibodies, we selected the conventional therapeutic radionuclide ^{131}I. Regardless, the evaluation of efficacy and safety profiles of RADCs must be conducted using advanced models, such as patient-derived xenograft models. Once successful RADCs are identified, they may be assessed for antigen-dependent toxicity in primate models. Finally, this novel class of drugs could advance to clinical trials for the treatment of CLDN18.2-positive cancers. These efforts would also pave the way for RADC-based therapeutics treating other cancers. The concurrent chemo-radiotherapy paradigm has resulted in a significant advancement in the treatment of locally advanced cancers.

Conclusion

In summary, the CLDN18.2 antibody-HLX58 was successfully radiolabeled with ^{125}I for microSPECT/CT imaging of CLDN18.2-expressing tumors. Additionally, the CLDN18.2-targeted RADC-^{131}I-HLX58-Der was successfully synthesized, demonstrating cytotoxic effects against CLDN18.2 positive tumor cells in vitro and showing efficacy in the

treatment of CLDN18.2-positive tumors in vivo. Considering that α-emitting radionuclides, such as ^{177}Lu, ^{225}Ac, ^{223}Ra, can be employed in the treatment of certain malignancies, they can also facilitate the synthesis of novel RADCs using appropriate labeling methods. Furthermore, considering the discovery of monoclonal antibodies targeting various molecules, numerous RADCs could be developed for the treatment of diverse cancer types.

Abbreviations

CLDN18.2, Claudin 18.2; ADC, antibody-drug conjugate; RADC, radio-antibody-drug conjugate; GGFG, glycynglycyn-phenylalanyn-glycyn; GC, gastric cancer; PBS, phosphate-buffered saline; TNR, target-to-nontarget tissue ratios; H&E, hematoxylin and eosin; IHC, immunohistochemistry.

Ethics Approval

The study was granted by the Ethics Committee of Fudan University Shanghai Cancer Center (No. 2019 Cancer Research JS-147).

Acknowledgments

The antibody HLX58 was generously provided by Henlius Biopharmaceutical Co., Ltd. We thank colleagues at our laboratory for helpful discussions in carrying out the studies.

Funding

This work was supported in part by National Key Research and Development Program of China (2020YFA0909003), The State Key Program of National Natural Science of China (U23A20465), The Science and Technology Commission of Shanghai Municipality (23DZ2291400), The National Natural Science Foundation of China (82272035), Shanghai Pujiang Program (22PJ1401700), National Isotope Engineering Technology Research Center Funding (GJTWSGCZX-202306), National Natural Science Foundation of China (82102097) and National Natural Science Foundation of China (12275057).

Disclosure

The authors report no conflicts of interest in this work.

References

1. Siegel RL, Miller KD, Fuchs HE, Jemal A. Cancer statistics. *CA Cancer J Clin*. 2021;71:7–33. doi:10.3322/caac.21654
2. Sung H, Ferlay J, Siegel RL, et al. Global cancer statistics 2020: GLOBOCAN estimates of incidence and mortality worldwide for 36 cancers in 185 countries. *CA Cancer J Clin*. 2021;71:209–249. doi:10.3322/caac.21660
3. Pennathur A, Gibson MK, Jobe BA, Luketich JD. Oesophageal carcinoma. *Lancet*. 2013;381:400–412. doi:10.1016/S0140-6736(12)60643-6
4. Qiu H, Cao S, Xu R. Cancer incidence, mortality, and burden in China: a time-trend analysis and comparison with the United States and United Kingdom based on the global epidemiological data released in 2020. *Cancer Commun*. 2021;41:1037–1048. doi:10.1002/cac2.12197
5. Wagner AD, Syn NL, Moehler M, et al. Chemotherapy for advanced gastric cancer. *Cochrane Database Syst Rev*. 2017;8:CD004064. doi:10.1002/14651858.CD004064.pub4
6. Korfer J, Lordick F, Hacker UT. Molecular targets for gastric cancer treatment and future perspectives from a clinical and translational point of view. *Cancers*. 2021;14:13. doi:10.3390/cancers14010013
7. Bass AJ, Thorsson V, Shmulevich I et al. Comprehensive molecular characterization of gastric adenocarcinoma. *Nature*. 2014;513:202–209. doi:10.1038/nature13480
8. Salem ME, Puccini A, Xiu J, et al. Comparative molecular analyses of esophageal squamous cell carcinoma, esophageal adenocarcinoma, and gastric adenocarcinoma. *Oncologist*. 2018;23:1319–1327. doi:10.1634/theoncologist.2018-0143
9. Wang J, Xiu J, Baca Y, et al. Large-scale analysis of KMT2 mutations defines a distinctive molecular subset with treatment implication in gastric cancer. *Oncogene*. 2021;40:4894–4905. doi:10.1038/s41388-021-01840-3
10. Hong JY, An JY, Lee J, et al. Claudin 18.2 expression in various tumor types and its role as a potential target in advanced gastric cancer. *Transl Cancer Res*. 2020;9:3367–3374. doi:10.21037/tcr-19-1876
11. Sahin U, Koslowski M, Dhaene K, et al. Claudin-18 splice variant 2 is a pan-cancer target suitable for therapeutic antibody development. *Clin Cancer Res*. 2008;14:7624–7634. doi:10.1158/1078-0432.CCR-08-1547
12. Juzeniene A, Stenberg VY, Bruland OS, Larsen RH. Preclinical and clinical status of PSMA-targeted alpha therapy for metastatic castration-resistant prostate cancer. *Cancers*. 2021;14:13.
13. Huang J, Agoston AT, Guo P, Moses MA. A rationally designed ICAM1 antibody drug conjugate for pancreatic cancer. *Adv Sci*. 2020;7:2002852. doi:10.1002/advs.202002852

14. Jain N, Smith SW, Ghone S, Tomczuk B. Current ADC linker chemistry. *Pharm Res*. 2015;32:3526–3540. doi:10.1007/s11095-015-1657-7
15. Shitara K, Bang YJ, Iwasa S, et al. Trastuzumab deruxtecan in previously treated HER2-positive gastric cancer. *N Engl J Med*. 2020;382:2419–2430. doi:10.1056/NEJMoa2004413
16. Bachir B, Anouti S, Abi JJ, et al. Evaluation of cardiotoxicity in HER-2-positive breast cancer patients treated with radiation therapy and trastuzumab. *Int J Radiat Oncol Biol Phys*. 2022;113:135–142. doi:10.1016/j.ijrobp.2021.12.159
17. Drago JZ, Modi S, Chandarlapaty S. Unlocking the potential of antibody-drug conjugates for cancer therapy. *Nat Rev Clin Oncol*. 2021;18:327–344. doi:10.1038/s41571-021-00470-8
18. Li Z, Guo X, Cao Z, et al. New MS network analysis pattern for the rapid identification of constituents from traditional Chinese medicine prescription Lishukang capsules in vitro and in vivo based on UHPLC/Q-TOF-MS. *Talanta*. 2018;189:606–621. doi:10.1016/j.talanta.2018.07.020
19. Ogitani Y, Aida T, Hagihara K, et al. DS-8201a, A novel HER2-targeting ADC with a novel DNA topoisomerase I inhibitor, demonstrates a promising antitumor efficacy with differentiation from T-DM1. *Clin Cancer Res*. 2016;22:5097–5108. doi:10.1158/1078-0432.CCR-15-2822
20. Dijoseph JF, Armellino DC, Boghaert ER, et al. Antibody-targeted chemotherapy with CMC-544: a CD22-targeted immunoconjugate of calicheamicin for the treatment of B-lymphoid malignancies. *Blood*. 2004;103:1807–1814. doi:10.1182/blood-2003-07-2466
21. Sievers EL, Appelbaum FR, Spielberger RT, et al. Selective ablation of acute myeloid leukemia using antibody-targeted chemotherapy: a Phase I study of an anti-CD33 calicheamicin immunoconjugate. *Blood*. 1999;93:3678–3684. doi:10.1182/blood.V93.11.3678
22. Sasso JM, Tenchov R, Bird R, et al. The evolving landscape of antibody-drug conjugates: in depth analysis of recent research progress. *Bioconjug Chem*. 2023;34:1951–2000. doi:10.1021/acs.bioconjchem.3c00374
23. Tamura K, Tsurutani J, Takahashi S, et al. Trastuzumab deruxtecan (DS-8201a) in patients with advanced HER2-positive breast cancer previously treated with trastuzumab emtansine: a dose-expansion, Phase 1 study. *Lancet Oncol*. 2019;20:816–826. doi:10.1016/S1470-2045(19)30097-X
24. Choy H, Macrae R. Irinotecan and radiation in combined-modality therapy for solid tumors. *Oncology*. 2001;15:22–28.
25. Keam SJ. Zolbetuximab: first Approval. *Drugs*. 2024;84:977–983. doi:10.1007/s40265-024-02056-x
26. Shitara K, Lordick F, Bang YJ, et al. Zolbetuximab plus mFOLFOX6 in patients with CLDN18.2-positive, HER2-negative, untreated, locally advanced unresectable or metastatic gastric or gastro-oesophageal junction adenocarcinoma (SPOTLIGHT): a multicentre, randomised, double-blind, Phase 3 trial. *Lancet*. 2023;401:1655–1668. doi:10.1016/S0140-6736(23)00620-7
27. Herrmann K, Schwaiger M, Lewis JS, et al. Radiotheranostics: a roadmap for future development. *Lancet Oncol*. 2020;21(3):e146–56. doi:10.1016/S1470-2045(19)30821-6
28. Jadvar H, Chen X, Cai W, Mahmood U. Radiotheranostics in cancer diagnosis and management. *Radiology*. 2018;286:388–400. doi:10.1148/radiol.2017170346
29. Sgouros G, Bodei L, Mcdevitt MR, Nedrow JR. Radiopharmaceutical therapy in cancer: clinical advances and challenges. *Nat Rev Drug Discov*. 2020;19:589–608. doi:10.1038/s41573-020-0073-9
30. D'Huyvetter M, Xavier C, Caveliers V, Lahoutte T, Muyldermans S, Devoogdt N. Radiolabeled nanobodies as theranostic tools in targeted radionuclide therapy of cancer. *Expert Opin Drug Deliv*. 2014;11:1939–1954. doi:10.1517/17425247.2014.941803
31. Dekempeneer Y, Keyaerts M, Krasniqi A, et al. Targeted alpha therapy using short-lived alpha-particles and the promise of nanobodies as targeting vehicle. *Expert Opin Biol Ther*. 2016;16:1035–1047. doi:10.1080/14712598.2016.1185412
32. Awad RM, Meeus F, Ceuppens H, et al. Emerging applications of nanobodies in cancer therapy. *Int Rev Cell Mol Biol*. 2022;369:143–199.
33. Wei W, Younis MH, Lan X, Liu J, Cai W. Single-domain antibody theranostics on the horizon. *J Nucl Med*. 2022;63:1475–1479. doi:10.2967/jnumed.122.263907